



Human HDAC isoform selectivity achieved via exploitation of the acetate release channel with structurally unique small molecule inhibitors

Lewis Whitehead*, Markus R. Dobler, Branko Radetich, Yanyi Zhu, Peter W. Atadja, Tavina Claiborne, Jonathan E. Grob, Andrew McRiner, Margaret R. Pancost, Anup Patnaik, Wenlin Shao, Michael Shultz, Ritesh Tichkule, Ruben A. Tommasi, Brian Vash, Ping Wang, Travis Stams

Novartis Institutes for Biomedical Research, 100 Technology Square & 250 Massachusetts Avenue, Cambridge, MA 02139, USA

ARTICLE INFO

Article history:

Received 1 April 2011

Revised 29 May 2011

Accepted 2 June 2011

Available online 15 June 2011

Keywords:

Histone deacetylase

X-ray crystallography

Selectivity

Acetate release hypothesis

Metal binding

ABSTRACT

Herein we report the discovery of a family of novel yet simple, amino-acid derived class I HDAC inhibitors that demonstrate isoform selectivity via access to the internal acetate release channel. Isoform selectivity criteria is discussed on the basis of X-ray crystallography and molecular modeling of these novel inhibitors bound to HDAC8, potentially revealing insights into the mechanism of enzymatic function through novel structural features revealed at the atomic level.

© 2011 Elsevier Ltd. All rights reserved.

1. Introduction

Histone deacetylases (HDACs) are an important class of enzymes involved in regulating chromatin unfolding, gene expression and DNA repair via histone acetylation and deacetylation processes. As such HDACs represent important therapeutic targets in anti-cancer^{1,2} as well as anti-viral, anti-parasitic and anti-inflammatory indications.³ HDACs are divided into three classes comprising Zn²⁺ cofactor dependent class I (HDAC1–3 and 8), class II (HDAC4–7, 9, 10), and the NADPH cofactor dependent class III (Sirtuins 1–7) whose primary function is deacetylation of lysine residues at the N-terminal of Histone domains 3 and 4. The majority of inhibitors currently being tested in the clinic were developed by academic and industrial laboratories targeting class I and II HDACs with non-selective, generally zinc chelating small molecules with liabilities including cross-reactivity and toxicity.^{4,5} There is evidence emerging that suggests that HDAC inhibitors, which specifically inhibit class I enzymes, offer distinct therapeutic advantage compared to the classical broad-spectrum inhibitors.^{6–13} However the high homology of the class I HDACs in the active site region and the 11 Å vertical channel promises to challenge any attempt to achieve isoform selectivity, when designing and developing novel therapeutic small molecule HDAC inhibitors. As previous molecular modeling

studies indicate, enzyme selectivity between HDAC1, 3 and 8 may be obtained by exploring the opening of the active site, however, differentiation between HDAC1 and 2 will be very difficult.¹⁴ We report the discovery of a new family of non-hydroxamate based, isoform selective, class I HDAC inhibitors capable of reaching into the acetate release channel deep within the enzyme and binding with novel zinc chelation.

In general HDAC inhibitors such as Trichostatin A (TSA, **1**) closely resemble the aliphatic acetyl-lysine substrate shown in Figure 1, and deliver a hydroxamic acid or another zinc binding group to the catalytic zinc cation. The metal cofactor is deeply buried in the narrow active site pocket, marking the intersection of the 11 Å vertical channel (acetyl-lysine binding tunnel) and the 14 Å horizontal channel (acetate release channel) as seen in co-crystal structures HDLP (HDAC-like protein),⁵ HDAH (HDAC-like amidohydrolase)¹⁵ and human HDAC8.¹⁶ All inhibitors consist of a zinc binding group and a polar capping group connected through a linker, preferably containing a vinylic or aryl group. In accordance with modeling predictions, previous medicinal chemistry attempts to generate the isozyme-specific HDAC inhibitors generally focused on varying the capping functionality or in a few cases the linker group.^{8,17}

Our investigation of a high throughput compound screening assay led to the discovery of a novel family (**2**) of non-hydroxamic acid containing class I HDAC inhibitors.¹⁸ These compounds are represented generically in structure **2** and exemplified as **3**, **4** in Figure 2. They have been found to exhibit a remarkable selectivity

* Corresponding author.

E-mail addresses: lewis.whitehead@novartis.com, lewlou1@verizon.net (L. Whitehead).

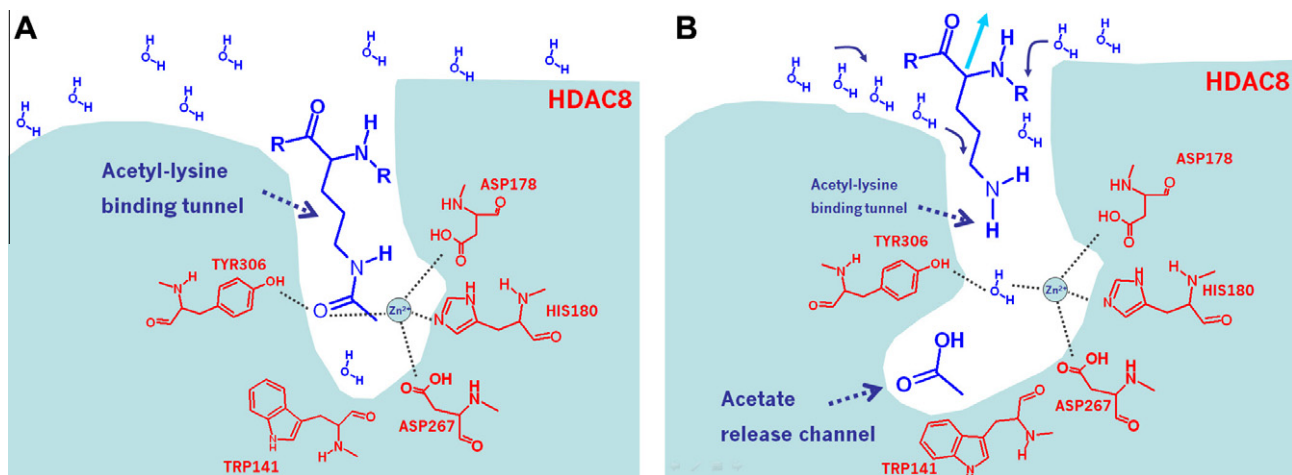


Figure 1. Schematic display of the HDAC enzymatic process. (A) Acetylated lysine binds into HDAC's binding tunnel coordinating with zinc, aspartic acid and tyrosine side-chains. R groups represent histone amino-acid chain (B) As lysine departs one would expect bulk-solvent water molecules to begin entering the tunnel, acetic acid is released into the acetate release channel.

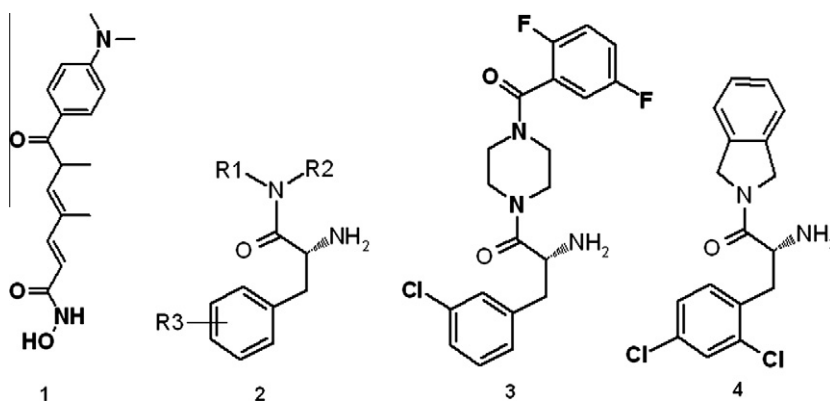


Figure 2. Histone deacetylase inhibitors; Trichostatin A (1); generic representation of the (R)- α -amino-ketone moiety 2; class I HDAC binding ligands 3, 4.

Table 1

Catalytic IC₅₀ values of the in vitro activity of 1, 3 and 4 in HDAC isoforms 1, 2, 6 and 8

Molecule	HDAC1	HDAC2	HDAC6	HDAC8 (nM)
1	3 nM	4 nM	51 nM	960
3	>30 μ M	>30 μ M	>30 μ M	200
4	1.7 μ M	3.9 μ M	>30 μ M	90

profile against class I HDAC isoforms, data that is shown in Table 1, which may be used to aid in understanding and modifying the molecular mechanisms connecting HDAC activity to cancer formation.

2. Results and discussion

HDAC8 is a member of the class I histone deacetylase enzyme family and is predominantly expressed in smooth muscle tissue. It has been implicated as a key player in the progression of cancers,¹⁹ and is therefore an enzymatic target of tremendous interest to laboratories around the world concerned with discovering a cure for these life threatening conditions. The most commonly recognized chemical class for inhibition of HDACi are the hydroxamic acids. These acids bind to the catalytic zinc cation at the base of the acetyl-lysine tunnel via an electrostatically favorable bi-dentate binding mode with two oxygen atoms, leaving the amide NH to form an additional hydrogen bonding interaction with a histidine.

In the clinic, hydroxamic acid containing therapeutics are proving to be effective in saving lives, for instance vorinostat²⁰ is FDA approved for use in T-cell lymphoma, with panobinostat²¹ and belinostat²² close to market approval. However, due to the metal chelating strength of the hydroxamic moiety, it is believed to be responsible for clinically observed side-effects such as nausea, thrombocytopenia, anemia and other metabolic abnormalities that are detrimental to the health of patients in contrast to their life-saving profile.²³ As such, the search for alternative small molecules containing weaker metal binding features has been of great interest to the HDAC community, as well as for the broader medicinal chemistry audience where metal binding chemical features are common in a variety of therapeutic siderophores,²⁴ protein,²⁵ RNA^{26,27} and DNA²⁷ targets in drug discovery.

In this manuscript the discovery of a novel chiral α -amino-ketone HDAC binding moiety is disclosed. The discussion will initially detail the nature of the chemical novelty, and then follow on with the details of co-crystallization of two closely related α -amino-ketone containing ligands within HDAC8. It will continue with the rationalization of isoform selectivity data and conclude with a speculative assessment of the mechanism of acetate release.

2.1. Small molecule structural novelty

The novelty of chelation to the catalytic zinc in HDAC8 with an α -amino-ketone motif is shown in Figure 3, the R chirality of the

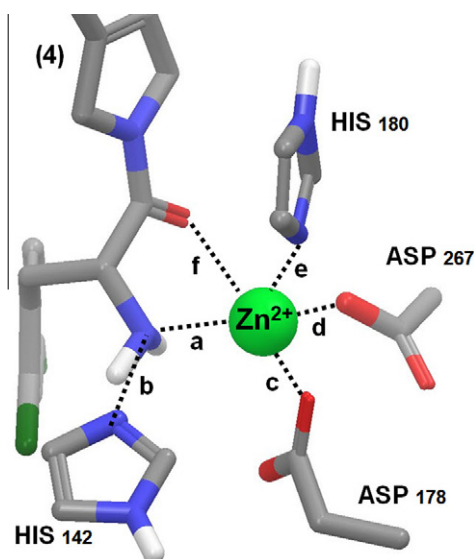


Figure 3. Novelty of the α -amino-ketone binding motif in HDAC8. $a = 2.2 \text{ \AA}$, $b = 2.9 \text{ \AA}$, $c = 2.0 \text{ \AA}$, $d = 2.0 \text{ \AA}$, $e = 2.3 \text{ \AA}$, $f = 2.95 \text{ \AA}$.

motif is essential. This binding feature has been experimentally observed in several complexes via inspection of small molecule X-ray crystal structure solutions within the Cambridge structural database.²⁸ In this database, reference code numbers ISODOJ and ISODUP,²⁹ MAFGUW,³⁰ MIVDEB,³¹ TEXTOF³² and TUFHEI³³ demonstrate the ability of the carbonyl oxygen and amine functionalities to coordinate with zinc, however in all but one (ISODOJ) of these examples the hydrogen bond donating capability of the amine is not observed, because it cannot be satisfied in these chemical complexes due to the absence of a suitable acceptor.

This zinc binding motif is accommodated in the presence of an uncharged amine. We suspect that during diffusion of **3** and **4** in their protonated state from the aqueous bulk solvent towards the HDAC enzymatic surface and the hydrophobic walls of the acetyl-lysine tunnel, that is, moving from a high to low dielectric physicochemical environment, de-protonation of the amine allows the α -amino-ketone moiety to perform this zinc binding pose. An alternative argument could be the basic His-142 extracts a proton which may be shuttled away from the binding area via the aspartic acid residues that are coordinating a site 1 mono-valent potassium cation.¹⁶

2.2. X-ray crystallography

X-ray crystal structures of HDAC8 in complex with compounds **3** and **4** were determined at 2.0 \AA and 2.7 \AA resolution, respectively. Figures 3 and 4 display the structures revealing a novel-binding mode in which the inhibitors make interactions with HDAC8 on both sides of the catalytic zinc cation, occupying volume in both the acetyl-lysine substrate tunnel and the acetate product release channel.

At the core of both molecules is a primary amine moiety that completes a pseudo-tetrahedral coordination with the active site zinc cation, which is also coordinated by protein residues Asp-178, His-180, and Asp-267. In addition, the central amino group donates a proton to the N(2) atom of His-142 forming a hydrogen bond. The adjacent carbonyl oxygen in **3** and **4** participate in a weakened electrostatic interaction with zinc at a distance of 2.8 \AA and 2.95 \AA , respectively in the structural complexes compared to 2.4 \AA for TSA. In addition, both species form a water-mediated hydrogen bond with the backbone amide of Gly-305.

The difluoro-benzyl-piperazine and the dihydro-isindole moieties of **3** and **4** perform *van der Waals* interactions with His-143, Gly-151, Phe-152, His-180 and Phe-208 of the acetyl-lysine substrate tunnel. A π -stack between the difluoro-benzyl-piperazine moiety of **3** and Phe-208 and T-stacking interactions of the dihydro-isindole in **4** with Phe-152 and Phe-208 are also noted. Novel inhibitor HDAC8 interactions are observed between the 3-chlorophenyl and the 2,4-dichlorophenyl moiety of compound **3** and **4**, respectively, with side-chains of Ile-34, Trp-141, Gly-303, Gly-304 and Tyr-306 of the acetate product release channel. More specifically, the phenyl rings of these molecules π -stack with the indole ring of Trp-141. These inhibitors differ from previously determined structures of HDAC8 (PDB codes 1T64, 3FOR) bound to hydroxamate inhibitors, such as TSA (**1**), in which interactions only take place at the active site zinc and acetyl-lysine substrate tunnel.¹⁶ To accommodate binding of **3** and **4** to the acetate release channel, the side chains of Trp-141, Phe-152 and Tyr-306 have an alternative geometry relative to the TSA(**1**)-HDAC8 protein-ligand complex. This side-chain movement is demonstrated in Figure 5. Additionally, second shell movements are also seen for Leu-31, Tyr-111, and Tyr-154.

Two monovalent potassium cations are also solved in this HDAC8 structural disclosure. Activation and inhibition of HDAC8 function with these cations has been experimentally validated.³⁴ A site 1 potassium ion resides approximately 7 \AA from the catalytic zinc, coordinated by Asp-176, Asp-178, His-180, Ser-199 and Leu-200. Site 2 potassium resides $\sim 15 \text{ \AA}$ from site 1, coordinated by Phe-189, Thr-192, Val-195, Tyr-225 and Ser-226.

2.3. Describing the binding data

To explain the inhibitory data of the molecules disclosed in Table 1, a series of homology models of HDAC1 were generated, multiple sequence alignments performed and X-ray crystallographic resources leveraged. Within HDAC8, molecule **4** ($M_w = 335.24 \text{ g/mol}$) has a ligand binding efficiency of 0.32 for this isozyme compared to 0.24 for compound **3** ($M_w = 441.41 \text{ g/mol}$), and an order of magnitude improved binding affinity over **1** ($M_w = 302.38 \text{ g/mol}$) with ligand efficiency of 0.27. In the acetate release channel the chlorophenyl moieties of **3** and **4** reside as shown in Figure 6, buried in a hydrophobic pocket flanked by residues described previously. It appears that **3** exploits more of a face-to-face phenyl moiety π -stacking interaction with Trp-141 than **4**, but the ortho substituted chloro of **4** exploits favorable hydrophobic pocket volume at the same time as influencing the shape of the benzylic functionality to place the *para*-chloro atom within 3.3 \AA of Ile-34 and 3.2 \AA of Arg-37. The *meta*-chloro on **3** reaches to within 3.8 \AA of Ile-34 and 4.1 \AA of the Arg-37 side-chain. This difference in proximity to the side-chain residues of Ile-34 and Arg-37 and the small difference in attractive *van der Waals* and coulombic forces that represents, is one rationalization for HDAC8 affinity of **3** and **4**, with compound **1** unable to exploit these favorable acetate release tunnel interactions in any way.

In the acetyl-lysine binding tunnel the piperazine and isindole moieties overlay as shown in Figures 4 and 6b. The difference in the hydrophobic nature of these compounds' interactions with Phe-152 and Phe-208 may simply be due to the presence of unfavorable polar piperazine nitrogen and carbonyl oxygen atoms for molecule **3** in comparison to more favorable apolar aromatic sp^2 carbons of molecule **4** exploiting this region of favorable hydrophobic binding volume. Also, a 29.4° difference in the χ_2 dihedral angle of Phe-152 between both structures provides **4** with a favorable T-shaped π -stacking interaction that **3** cannot form. In Figure 7 the overlay of the HDAC8-**3** complex with recently solved structures of HDAC8-compound **1** (PDB code 3FOR) and HDAC8-substrate

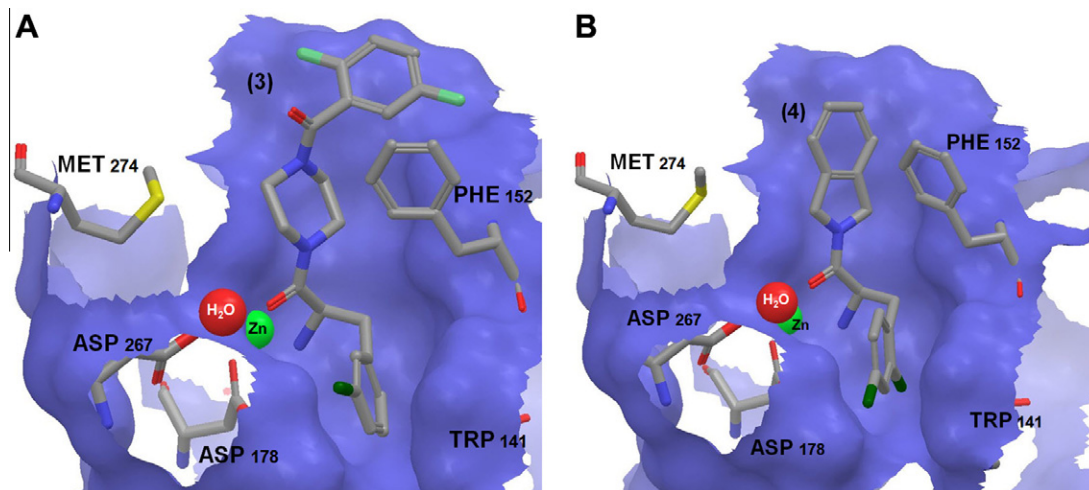


Figure 4. (A) Position of **3** in the active site of HDAC8. (B) Position of **4** in the active site of HDAC8.

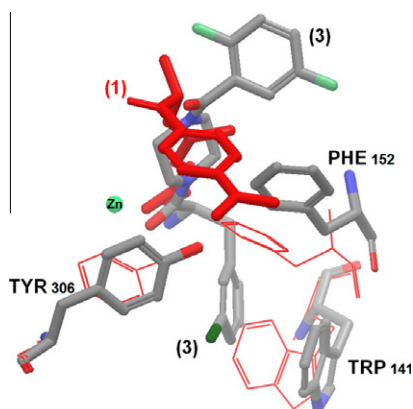


Figure 5. Overlay of **1** and **3** illustrating movement of residues Tyr-306, Trp-141 and Phe-152 to accommodate **3** penetrating into the acetate release tunnel.

(PDB code 3EWF)³⁵ shows the proximity of the positioning of the difluorophenyl fragment to loop 2 residues, specifically Asp-101 for which we were unable to determine the atomic coordinates. In this alignment Asp-101 and the difluorophenyl moiety are steric

clashing, suggesting that loop 2 movement is altered in such a way that **3** may have modified $K_{on/off}$ binding rate behavior in relation to **4** because the acetyl-lysine tunnel will be more open and thus exposed to the solvent accessible surface. Note the positioning of Phe-152 between HDAC8 structures, if Asp-101 is un-impeded, the benzylic amino-acid side chain of Phe-152 sits deeper within the acetyl-lysine binding tunnel. As **4** does not exploit the solvent exposed rim of HDAC8, it clearly avoids steric clashing with mobile side-chains like Asp-101 at the surface of the enzyme, stabilizing the tunnel wall resulting in stronger HDAC8 binding affinity.

2.4. HDAC1 and 2

The observed motion of the loop 2 amino-acid side-chain residues at the HDAC solvent accessible surface, combined with side-chain differences in the acetate release channel, can explain the binding behavior of **3** and **4** with HDAC1. A 1.7 μM binding affinity for **4** in HDAC1 is evidence for the formation of the acetate release channel we have described in HDAC8. The most prominent amino-acid differences between HDAC8 and HDAC1 in this channel are Trp-141 to leucine and Ile-34 to lysine shown in Figure 8, creating a smaller channel area available for binding. The loss of favorable π -stacking interactions between phenyl rings due to the absence

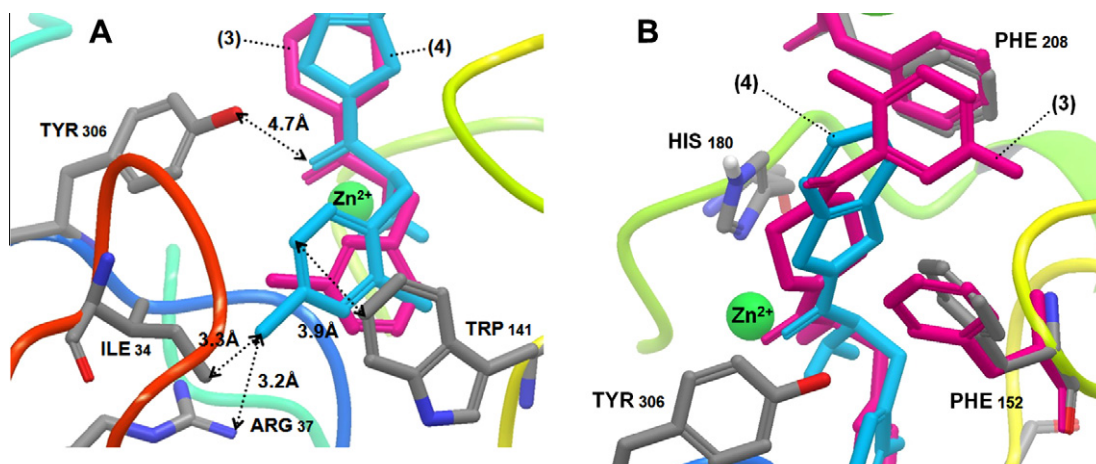


Figure 6. Alignment of **3** and **4** with prominent amino-acid interactions. (A) Acetate release channel close contacts, complex **3** shown in magenta, **4** is in light blue. (B) Movement of the benzylic rotamer of the Phe-152 side-chain between crystallographic coordinates.

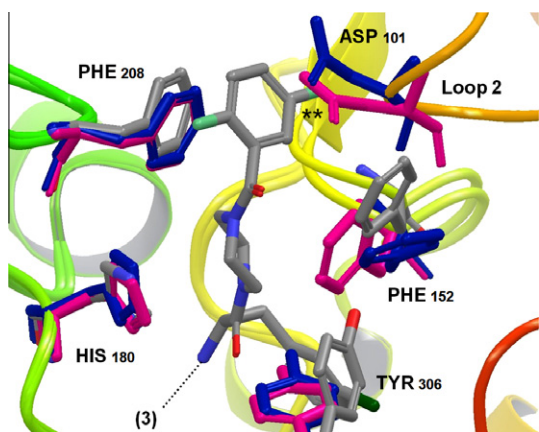


Figure 7. Alignment of the HDAC8-ligand **3** complex with published HDAC8 PDB structures. Magenta and dark blue side chains of Asp-101, Phe-152, His-180, Phe-208 and Tyr-306 correspond to HDAC8 complexes with PDB codes 3EWF and 3FOR, respectively. Note the proximity of the fluorophenyl moiety with the acidic Asp-101 side-chains identified by the asterisks.

of the indole side-chain of Trp-141, along with the longer lysine side-chain probing deeper into the channel towards the catalytic zinc will be detrimental to ligand binding and cause for loss in binding affinity for **4** in relation to its HDAC8 activity of 90 nM. HDAC1 data for **3** suggests that interactions within the acetyl-lysine binding tunnel and the solvent accessible surface are responsible for the complete lack of activity. Asp-101 in HDAC8 is Asp-99 in HDAC1, and as our previous discussion details, the difluorophenyl group of **3** is unlikely to fit comfortably in HDAC1 or the motion of loop 2 halts this molecule's progression into the HDAC1 active site completely as the IC₅₀ data reports.

Data for the HDAC2 enzyme suggests molecule **4** is capable of accessing the acetate release channel for this isozyne, binding with an IC₅₀ of 3.9 μM. As the sequence homology between HDAC1 and 2 is 83%, there is little evidence in the surrounding atomic binding neighborhood of compound **4** to explain the minor disparity in this structure activity relationship between HDAC isozymes 1 and 2, IC₅₀ values that are relatively similar for binding to both enzymes. The IC₅₀ data for compound **1** suggests that the atomic environment it experiences with HDAC1 is essentially equivalent in HDAC2, which is supported by the knowledge that amino-acid

residue differences between isozymes are distant from the active site.

2.5. The class IIb HDAC isoform HDAC6

HDAC6 is a class IIb histone deacetylase with 19.7% sequence identity with HDAC1.⁵ Trichostatin A (**1**) IC₅₀ binding data to HDAC6 implies that the acetyl-lysine binding tunnel and the catalytic zinc areas are structurally similar to the class I HDAC1 and 2 isozymes because the data is consistently below the 100 nM mark. The acetate release channel in HDAC8 is formed with amino-acid side chains from loops 1, 2, 3 and 7. On inspecting the molecular models of the HDAC1/8 channels and the published sequence identity to HDAC6⁵ a number of interesting observations are evident. For instance comparing HDAC6 to HDAC1 primary amino-acid sequences, loop 1 is one amino-acid shorter, whereas loops 2 and 3 are four and two residues shorter, respectively. The shorter length of the HDAC6 loops will effect the cavity shape and physicochemical nature of the acetate release channel, and consequently the selectivity data we observe. Also, residues Leu-137 in HDAC1 and Trp-141 in HDAC8 have no equivalent residue in the HDAC6 sequence as this position is within a two residue gap in the alignment shown by Finnin et al. Indeed in order for His-210 in HDAC6 to retain a zinc binding contact, Gly-209 would occupy the position of Leu-137 in HDAC1 with very little offered in terms of favorable intramolecular interactions for the substituted benzylic functionalities of molecules **3** and **4**. In addition, Arg-98 in the HDAC6 loop 1 would be the equivalent residue to Lys-24 in HDAC1, and Ile-34 in HDAC8. It has already been noted for HDAC1 that the inclusion of a basic amino-acid in the acetate release channel is likely to be detrimental to the binding data shown for molecule **4**. HDAC6 selectivity is clearly demonstrated in the SAR, however we are unable to provide evidence at this time that synthetic modifications to this novel family of HDAC binders are capable of activity on HDAC6, but suspect that the acetate release channel has a unique three dimensional geometry yet to be determined and chemically exploited.

2.6. Mechanism of acetate release

A comparison of the size and shape of the internal acetate release channel observed in HDAC8 with the HDLP structural homology may have revealed more insights into the mechanism of acetate

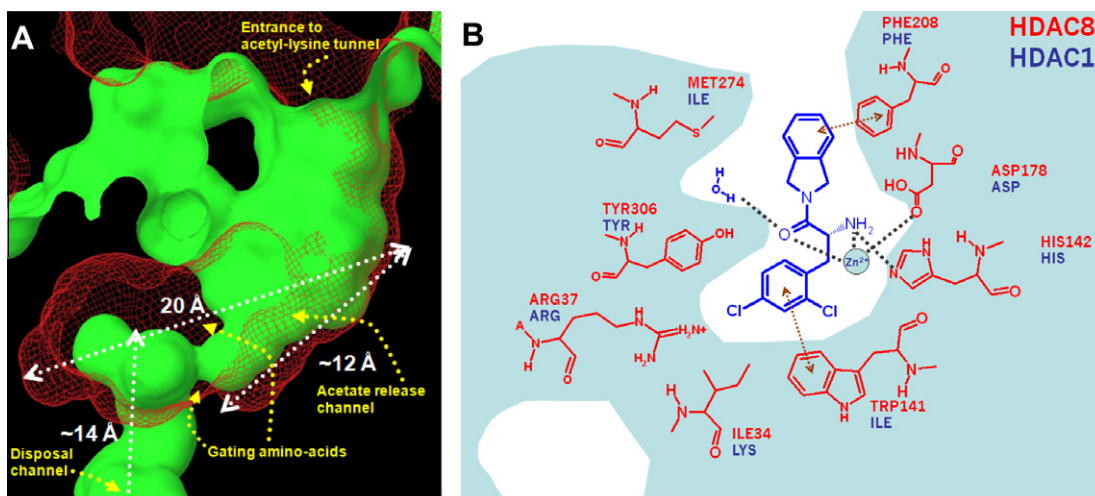


Figure 8. Prominent amino-acid side-chain differences between HDAC8 (magenta) and HDAC1 in the acetate-release channel. Crystal structure coordinates of the HDAC8-ligand **4** complex aligned with an HDAC1 homology model.

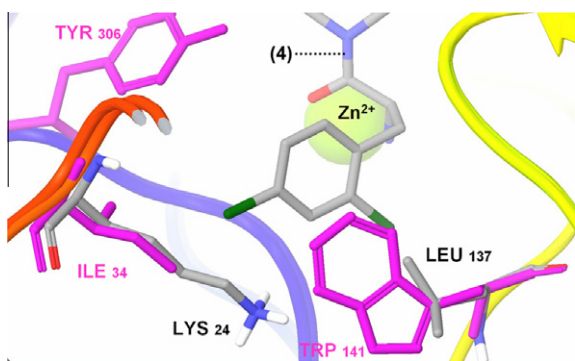


Figure 9. (A) A comparison between the published HDLP acetate release channel (red mesh with foreground clipped for clarity), with this reported HDAC8 structure (green solid surface). Measurement criteria discussed in [Supplementary data](#). Gating amino-acid residues are defined as Leu-31, Ile-34, Arg-37, Ser-138 and Trp-141. (B) Schematic of **4** within HDAC8 showing key binding interactions and the amino-acid side-chain environment in HDAC1/8.

release from histone deacetylases. These authors note that the origin of the measurement criterion of the internal 14 Å channel has not been reported. For instance the distance between the amino-acids that define the start and end of the channel (terminal hydroxyl functionality on Ser-29 and His-131 imidazole side-chain) is ~20 Å for the first HDLP reported structure.⁵ In [Figure 9](#) we compare the shape of the '14 Å' acetate release channel between HDLP and HDAC8. Notice that the volume available in the HDAC8 acetate release channel is considerably smaller than HDLP. There are clearly two volume components in HDAC8, and this internal acetate release channel cavity appears to be divided at a junction between amino-acid residues Leu-31, Ile-34, Arg-37, Ser-138 and Trp-141 into an '12 Å+14 Å' channel pair.

The existence of the 12 Å+14 Å channel arrangement leads us to speculate about the mechanism of acetate release within HDACs. In [Figure 1b](#) the re-population of the acetyl-lysine tunnel with water molecules from the solvent accessible surface is an assumption. On approach of another acetylated lysine histone residue one could speculate that the active diffusional forces at play at the molecular level shunt the acetic acid product from the previous enzymatic event from the 12 Å 'release' channel into the 14 Å 'disposal' channel. In this process Arg-37 would play a role in charge stabilization of the acetic acid and in partnership with Trp-141 relocating the side-chain indole moiety to close the 12 Å channel, both residues

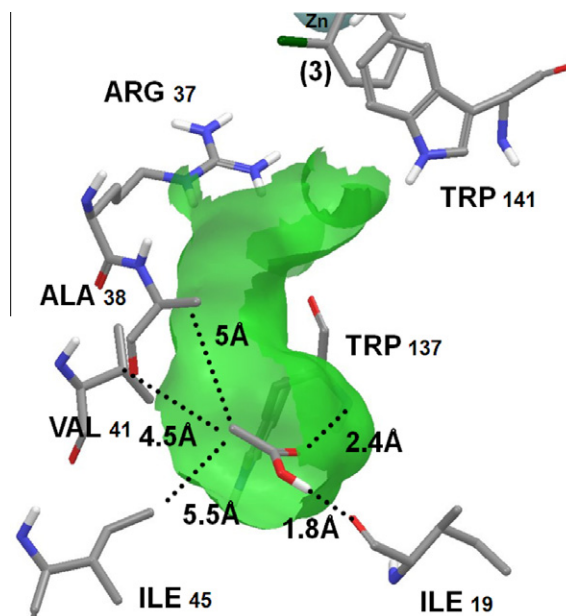


Figure 11. A proposed docking mode of acetic acid released from the previous catalytic cycle transferred into the 14 Å disposal channel. H-Bonding and hydrophobic matching distances are noted, with a transparent contour of the channel shown in green. Compound **3** and zinc are also displayed.

are responsible for actively transporting the acid into the second channel. [Figure 10](#) is a schematic of the process we describe with acetic acid switching between channels in order for HDAC to prepare for another catalytic cycle. As a further curiosity, a molecular docking experiment with acetic acid was completed to assess the likelihood of the 14 Å disposal channel accommodating this chemical species, the result of which is shown in [Figure 11](#).

The acetic acid settles well at the base of the 14 Å disposal channel making hydrogen bonding contact with Ile-19 and Trp-137. The acidic species also makes favorable hydrophobic contacts via its methyl group with the side-chain residues of Ile-45, Ala-38 and Val-41. This may indicate the final resting place of the acetic acid group within the histone deacetylase prior to its release via a mechanism mediated between residues Tyr-20, Ala-38, Val-41 and His-42 whose side-chain residues separate the acetic acid moiety in this disposal cavity from the aqueous bulk solvent as shown in [Figure 12](#).

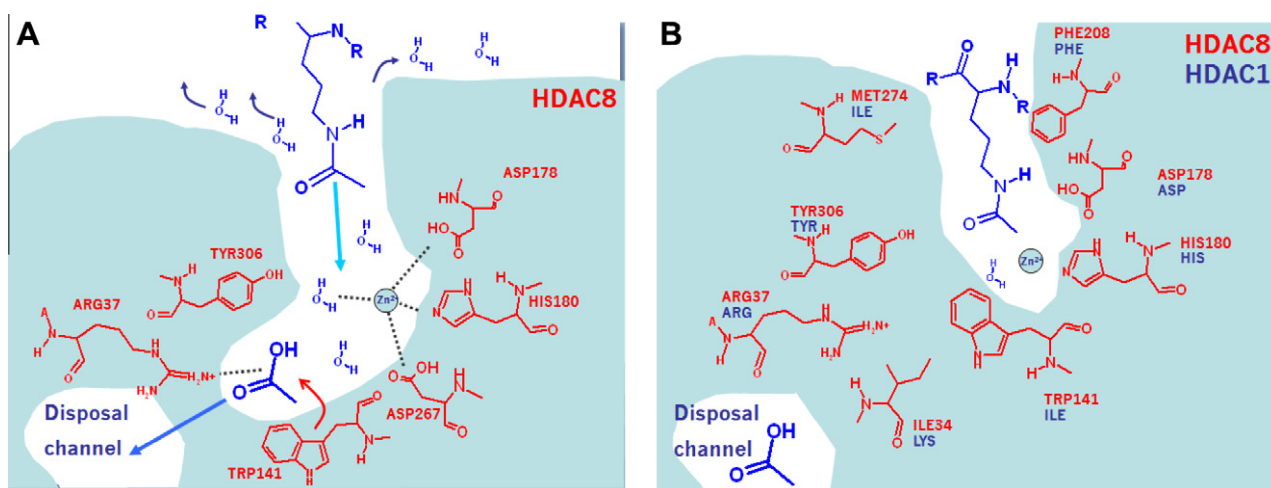


Figure 10. A proposed mechanism of HDAC8 catalytic behavior. (A) Acetylated lysine re-occupies the tunnel along with water (B) acetic acid released from the previous catalytic cycle is transferred into the 14 Å 'disposal' channel.

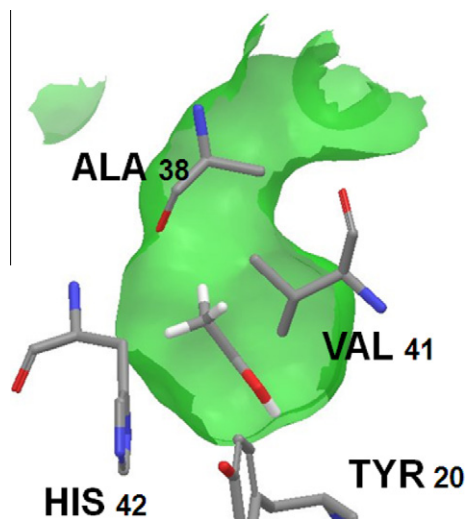


Figure 12. The proposed docking mode of acetic acid in the 14 Å disposal channel. Transparent green contour of the disposal channel has been clipped in the foreground to aid visualization. Tyr-20, Ala-38, Val-41 and His-42 form the barrier between the interior of the enzyme and the exterior solvent.

3. Conclusions

The hereby-presented novel binding mode of an isoform selective, non-hydroxamic acid containing inhibitor of class I human histone deacetylase isoforms is presented. This chemical functionality may also provide useful as an alternative metal-binding war-head motif for other targets of interest to practitioners of small molecule drug-discovery. Implications and full exploration of our recent findings for the design of isoform selective histone deacetylase inhibitors for the treatment of anti-cancer and anti-parasitic disease indications shall be disclosed and discussed in full account in a future communication.

4. Methods

4.1. HDAC fluorescence assay for IC₅₀ determination

All reaction components are prepared in fluorescent assay buffer (25 mM Tris-HCl, pH 8.0, 137 mM NaCl, 2.7 mM KCl, 1 mM MgCl₂). Add HDAC enzyme (fivefold activity) and diluted inhibitors (total volume is 25 μl) to clear bottom 96-well isoplate. Initiate reactions by adding 25 μl Rhodamine substrate (15 μM for the HDAC1 and 2 assay, 8 μM for HDAC6 and 8 assay). The background well contains panobinostat at 30 μM to completely inhibit HDAC enzyme activity. Enzyme reactions with DMSO are used as positive control. The reaction is run for 1 h at 37 °C and stopped with 50 μl/well of developer (1.35 mg/ml Trypsin) with TSA(1). Develop at room temperature for 10 min and read plate with Cytofluor Fluorescence Reader at excitation 485 nm and emission 530 nm.

4.2. Expression and protein purification

The gene for human HDAC8 was cloned into the pFastbacHTB vector (Invitrogen) and a high titer *baculo* virus was obtained using the Bac-to-Bac system (Invitrogen). *Spodopterafrugiperda*, Sf9, cells were infected with the *baculo* virus containing the full length HDAC8 with an N terminal hexahistidine tag followed by a TEV cleavage site for 65 h. Forty grams of frozen sf9 cell pellet was resuspended in 200 ml of room temperature lysis buffer (100 mM TRIS pH 8, 250 mM KCl, 10 mM zinc acetate, 1 mM TCEP) by stirring for 10 min at 4 °C. The cells were lysed by sonication for 5 min at

50% power at 50% duty cycle, and clarified by centrifugation at 200,000g at 4 °C for 1 h. The supernatant was batch bound onto 3 ml of Ni Sepharose High Performance resin (GE) that was pre-equilibrated in lysis buffer for 1 h at 4 °C. Resin was washed with lysis buffer plus 5 mM imidazole, and protein eluted with 250 mM imidazole. Following elution the sample was cleaved with AcTev protease (Invitrogen) yielding full length HDAC8 with an extra 5 N terminal amino acids of GAMGS. The cleaved sample was further purified on a Mono Q 10/100 GL column (GE) pre-equilibrated in buffer A (20 mM TRIS pH 8, 100 mM KCl, 1 mM TCEP), protein was eluted using a 20 column volume gradient to 1 M KCl. The fractions containing HDAC8 were pooled and assayed for zinc content using the colorimetric chelator 4-(2-pyridylazo)resorcinol, PAR.³⁶ The zinc content was adjusted by adding zinc acetate to 1.5-fold the HDAC8 concentration and incubating for 15 min at room temperature followed by a cleanup of excess zinc with EDTA. The zinc loaded HDAC8 was purified by size exclusion on a Superdex 75 26/60 prep grade column (GE) which was equilibrated in SEC buffer (20 mM TRIS pH 8, 50 mM NaCl, 50 mM KCl, 50 mM ammonium acetate, 1 mM TCEP). The final yield of HDAC8 was 66 mg and the purity was estimated to be greater than 98%. The zinc content of the purified HDAC8 was measured to be 1 zinc per protein molecule.

4.3. Chemistry. Methods and materials

1-Hydroxybenzotriazole (HOBT), *N*-ethyl-*N'*-(3-dimethylaminopropyl)carbodiimide hydrochloride (EDC-HCl), diisopropylethylamine (DIEA) and isoindoline were purchased from Sigma-Aldrich and used as such. BOC-3-chloro-*D*-phenyl alanine and BOC-2,4-dichloro-*D*-phenylalanine were purchased from Chem-Impex. Trichostatin A (**1**) was purchased from Sigma-Aldrich. ¹H and ¹³C NMR spectra were recorded on Bruker Avance 400, equipped with BBO 5 mm NMR probe, operating at frequency of 400 MHz for ¹H and 100 MHz for ¹³C. All chemical shifts were referenced to standard frequency of SiMe₄ set at 0 ppm. High resolution mass spectra were recorded using Agilent 1100 HPLC system (5–95% acetonitrile in water, 0.1% formic acid gradient, using Intersil ODS3 C18 column).

4.3.1. (*R*)-2-Amino-1-[4-(2,5-difluoro-benzoyl)-piperazin-1-yl]-3-(3-chloro-phenyl)-propan-1-one (**3**)

To the solution of BOC-3-chloro-*D*-phenylalanine (0.10 g, 0.340 mmol) in dichloromethane (1.2 mL) were added EDC.HCl (0.074 g, 0.387 mmol), HOBT (0.059 g, 0.387 mmol) and DIEA (0.162 ml, 0.928 mmol) at 0 °C under nitrogen atmosphere. The solution was stirred for 15 min and (2,5-difluoro-phenyl)-piperazin-1-yl-methanone³⁷ (0.070 g, 0.309 mmol) was added. After 16 h, reaction mixture was diluted with 25 mL of dichloromethane and washed with 25 mL of satd NaCl solution. Organic layer was separated, dried using MgSO₄ and solvent was removed under reduced pressure. Resulting crude was purified using flash column chromatography (10–90% ethyl acetate/hexanes) to afford the desired coupled product (0.144 g, 92% yield). Purified product (0.140 g, 0.276 mmol) was dissolved in dichloromethane (1 mL) and to clear solution was added 4 M HCl in dioxane (1.723 ml, 6.89 mmol) via a syringe. Solution was stirred for 16 h. Upon completion of reaction, solvent was removed under reduced pressure, and resulting crude was crystallized using ethyl acetate/hexanes mixture to afford the title compound **3** (0.095 g, 85% yield). ¹H NMR (400 MHz, CD₃OD): δ 2.98–3.25 (m, 5H), 3.30–3.41 (m, 1H), 3.43–3.51 (m, 1H), 3.52–3.74 (m, 3H), 4.54–4.77 (m, 1H), 7.12–7.41 (m, 7H) ¹³C NMR (100.6 MHz, CD₃OD): δ 38.1, 42.6, 42.7, 42.8, 43.5, 46.1, 46.6, 47.5, 47.6, 51.8, 116.5, 116.7, 118.6, 118.7, 118.8, 118.9, 119.6, 119.7, 119.8, 119.9, 129.4, 130.9, 131.8, 135.9, 137.7, 154.3, 156.7, 158.9, 161.5, 165.9, 168.3 HRMS

(TOF-MS) Exact mass calcd for $C_{20}H_{20}ClF_2N_3O_2$ $[M+H]^+$; 408.1290, found: 408.1292.

4.3.2. (R)-2-Amino-3-(2,4-dichloro-phenyl)-1-(1,3-dihydro-isoindol-2-yl)-propan-1-one (4)

To a stirred solution of Boc-2,4-dichloro-D-phenylalanine (0.280 g, 0.84 mmol), EDC·HCl (0.161 g, 0.84 mmol), HOBT (0.170 g, 1.26 mmol) and DIPEA (1.12 mL, 6.29 mmol) in DMF (2.0 mL), isoindoline (0.10 g, 0.84 mmol) was added. The reaction was stirred at room temperature for 24 h. Upon completion, solvent was removed under reduced pressure and the crude was purified using column chromatography to provide desired coupled product in 78% yield. To the purified compound (0.21 g, 0.48 mmol) was added 1 M HCl (9.5 mL, 1 M in Et₂O). After 4 h of stirring, the solvent was removed under reduced pressure to afford target compound **4** as a white solid. ¹H NMR (400 MHz, CD₃OD): δ 3.42 (d, 2H, 8.0 Hz), 4.24 (d, 1H, 12 Hz), 4.63 (t, 1H, 8.0 Hz), 4.72 (d, 1H, 16 Hz), 4.89 (d, 1H, 16 Hz), 5.00 (d, 1H, 12 Hz), 7.26 (m, 1H), 7.35 (m, 4H), 7.44 (d, 1H, 8.0 Hz), 7.54 (d, 1H, 4.0 Hz) ¹³C NMR (100.6 MHz, CD₃OD): δ 35.3, 52.1, 53.2, 53.6, 123.7, 123.9, 128.9, 129.1, 129.2, 130.7, 132.1, 132.4, 136.0, 136.3, 136.4, 136.6, 168.1 HRMS (TOF-MS) Exact mass calcd for $C_{17}H_{16}Cl_2N_2O$ $[M+H]^+$; 335.0718, found: 335.0712.

4.4. Crystallization and structure determination

HDAC8–inhibitor complexes were formed by incubating HDAC8 at 25 mg/mL with either 1 mM compound **1** or **2** for 1 h at 4 °C. Crystals of HDAC8–inhibitor complexes grew within one week by hanging drop vapor diffusion using 2 μl complex + 2 μl well solution over 1 ml of well solution (100 mM TRIS pH 8, 12–15% PEG 3350, 500 mM NDSB-201, 18% isopropanol). The crystals were cryo-protected with the addition of 15% glycerol and 1 mM compound for 5–10 min at 4 °C prior to flash freezing in liquid nitrogen.

Diffraction data for the HDAC8-inhibitor **3** crystals were collected on a Saturn92 CCD detector using Cu-Kα radiation ($l = 1.5418$) from a Rigaku FR-E microfocussing rotating anode X-ray generator operating at 45 kV and 45 mA, with Varimax optics. Diffraction data for the HDAC8-inhibitor **4** crystals were collected on the IMCA 17BM line at the Advanced Proton Source (APS, Argonne National Laboratory). Each data set was measured from a single crystal and the reflections were indexed, integrated, and scaled using the HKL2000 package.³⁸ The space group for each HDAC8–inhibitor complex was $P2_1$ with 1 HDAC8–inhibitor complex in the asymmetric unit. Molecular replacement was performed using PHASER³⁹ with the initial model of HDAC8-TSA complex (PDB entry 1T64) with the water, ion, and inhibitor molecules removed. Structure determination was achieved through iterative cycles of both positional and simulated annealing refinement using CNX⁴⁰ or BUSTER⁴¹ and model building using Coot⁴² Individual B-factors were refined using an overall anisotropic B-factor refinement along with bulk solvent correction. The inhibitors along with solvent and ion molecules were built into the model in later rounds of refinement. The final coordinates for HDAC8 contain residues Leu-14-Ser-83 (or Glu-85 in cpd **3** structure) and Gly-107-Val-377, the N-terminal 13 residues and the loop containing Gln-84-Glu-106 were not modeled due to lack of electron density. Data collection and refinement statistics are shown in Table 2.

4.5. Computational methods

Homology protein models of HDAC1 and 2 were generated with the PRIME algorithm, molecular docking with Glide and cavity exploration with SiteMap, all of which reside in the Maestro suite of applications,⁴³ using HDAC8 X-ray crystallographically determined coordinates from this study and the published work of

Table 2
Crystallographic data, phasing and refinement information

Molecule	3	4
Space group	$P2_1$	$P2_1$
Unit cell	$a = 57.81 \text{ \AA}$ $b = 53.67 \text{ \AA}$ $c = 61.34 \text{ \AA}$ $\alpha = \gamma = 90^\circ$ $\beta = 108.99^\circ$	$a = 57.64 \text{ \AA}$ $b = 53.37 \text{ \AA}$ $c = 60.89 \text{ \AA}$ $\alpha = \gamma = 90^\circ$ $\beta = 109.47^\circ$
Resolution range (Å)	29.06–2.00	29.82–2.70
Total observations	86,153	35,430
Unique reflections	23253	8238
Completeness (%) ^a	99.6 (97.9)	100.0 (100.0)
I/σ^a	11.3 (1.8)	12.3 (2.8)
$R_{\text{sym}}^{a,b}$	0.071 (0.293)	0.159 (0.469)
$R_{\text{cryst}}/R_{\text{free}}^c$	0.177/0.221	0.179/0.244
Protein atoms	2663	2673
Heterogen atoms	31	25
Solvent molecules	234	183
Average B-factor (Å ²)	27.5	24.4
<i>Rms deviations from ideal values</i>		
Bond lengths (Å)	0.010	0.004
Bond angle (°)	1.03	0.7

^a Numbers in parenthesis are for the highest resolution shell.

^b $R_{\text{sym}} = \sum |I_h - \langle I_h \rangle| / \sum I_h$ over all h , where I_h is the intensity of reflection h .

^c R_{cryst} and $R_{\text{free}} = \sum ||F_o| - |F_c|| / \sum |F_o|$, where F_o and F_c are observed and calculated amplitudes, respectively. R_{free} was calculated using 5% of data excluded from the refinement.

external research groups.^{35,44} Sequence alignments were performed with ClustalW⁴⁵ and used alongside published HDAC alignments to verify PRIME's assessment of amino-acid sequence matching prior to model building. Structural alignments were performed with the protein alignment feature in Maestro and internally and externally available protein–ligand X-ray crystal structures were accessed with Proasis software.⁴⁶

Acknowledgments

Use of the IMCA-CAT beam-line 17-BM at the Advanced Photon Source was supported by the companies of the Industrial Macromolecular Crystallography Association through a contract with the Center for Advanced Radiation Sources at the University of Chicago. Use of the Advanced Photon Source was supported by the US Department of Energy, Office of Science, Office of Basic Energy Sciences, under Contract No. W-31-109-Eng-38.

T.C. is a B³ baccalaureate student shared between the Massachusetts Institute of Technology and N.I.B.R., funded through the N.I.B.R. Diversity and Inclusion Office. L.W. and T.S. would like to thank Chris Harwell, Steven Litster, Michael Derby and Michael Steeves of NIBR IT for Linux hardware maintenance and software installation support. L.W. thanks 2010 Seeding Labs visiting fellow Dr. Evans Ogwagwa of Kenyatta University in Nairobi for enlightening HDAC discussions.

Supplementary data

Supplementary data (atomic coordinates for HDAC8 in complex with inhibitors **3** and **4** have been deposited in the Protein Data Bank with accession codes 3SFF and 3SFH, respectively. Additional images are contained) associated with this article can be found, in the online version, at doi:10.1016/j.bmc.2011.06.030.

References and notes

1. Cho, Y. S.; Whitehead, L.; Li, J.; Chen, C. H.; Jiang, L.; Vögtle, M.; Francotte, E.; Richert, P.; Wagner, T.; Traebert, M.; Lu, Q.; Cao, X.; Dumotier, B.; Fejzo, J.; Rajan, S.; Wang, P.; Yan-Neale, Y.; Shao, W.; Atadja, P.; Shultz, M. J. *Med. Chem.* **2010**, *53*, 2952.

2. (a) Grozinger, C. M.; Schreiber, S. L. *Chem. Biol.* **2002**, *9*, 3; (b) Marks, P.; Rifkind, R. A.; Richon, V. M.; Breslow, R.; Miller, T.; Kelly, W. K. *Nat. Rev. Cancer* **2001**, *1*, 194; (c) Miller, K. M.; Tjeertes, J. V.; Coates, J.; Legube, G.; Polo, S. E.; Britton, S.; Jackson, S. P. *Nat. Struct. Mol. Biol.* **2010**, *17*, 1144.
3. (a) Meineke, P. T.; Liberator, P. *Curr. Med. Chem.* **2001**, *8*, 211; (b) Shestakova, E.; Bandu, M. T.; Dolly, J.; Bonnefoy, E. *J. Virol.* **2001**, *75*, 3444; (c) Ito, K.; Ito, M.; Elliot, M. W.; Cosio, B.; Caramori, G.; Kon, M. O.; Barczyk, A.; Hayashi, S.; Adcock, I. M.; Hogg, C. J.; Barnes, J. P. *N. Eng. J. Med.* **2005**, *352*, 1967; (d) Mukherjee, P.; Pradhan, A.; Shah, F.; Tekwani, B. L.; Avery, M. *Bioorg. Med. Chem.* **2008**, *16*, 5254.
4. Yoshida, M.; Kijima, M.; Aktia, M.; Beppu, T. *J. Biol. Chem.* **1990**, *265*, 17174.
5. Finnin, M. S.; Donigan, J. R.; Cohen, A.; Richon, V. M.; Rifkind, R. A.; Marks, P. A.; Breslow, R.; Pavletich, N. P. *Nature* **1999**, *401*, 188.
6. Karagiannis, T. C.; El-Osta, A. *Leukemia* **2007**, *21*, 61.
7. Tang, W.; Luo, T.; Greenberg, E. F.; Bradner, J. E.; Schreiber, S. L. *Bioorg. Med. Chem. Lett.* **2011**, *21*, 2601.
8. Bieliauskas, A. V.; Pflum, M. K. *Chem. Soc. Rev.* **2008**, *37*, 1402.
9. Estiu, G.; West, N.; Mazitschek, R.; Greenberg, E.; Bradner, J. E.; Wiest, O. *Bioorg. Med. Chem.* **2010**, *18*, 4103.
10. Bertrand, P. *Eur. J. Med. Chem.* **2010**, *45*, 2095.
11. Moradei, O. M.; Mallais, T. C.; Frechette, S.; Paquin, I.; Tessier, P. E.; Leit, S. M.; Fournel, M.; Bonfils, C.; Trachy-Bourget, M. C.; Liu, J. H.; Yan, T. P.; Lu, A. H.; Rahil, J.; Wang, J.; Lefebvre, S.; Li, Z. M.; Vaisburg, A. F.; Besterinan, J. M. *J. Med. Chem.* **2007**, *50*, 5543.
12. Witter, D. J.; Harrington, P.; Wilson, K. J.; Chenard, M.; Fleming, J. C.; Haines, B.; Kral, A. M.; Secrist, J. P.; Miller, T. A. *Bioorg. Med. Chem. Lett.* **2008**, *18*, 726.
13. Methot, J. L.; Chakravarty, P. K.; Chenard, M.; Close, J.; Cruz, J. C.; Dahlberg, W. K.; Fleming, J.; Hamblett, C. L.; Hamill, J. E.; Harrington, P.; Harsch, A.; Heidebrecht, R.; Hughes, B.; Jung, J.; Kenific, C. M.; Kral, A. M.; Meinke, P. T.; Middleton, R. E.; Ozerova, N.; Sloman, D. L.; Stanton, M. G.; Szewczak, A. A.; Tyagarajan, S.; Witter, D. J.; Paul-Secrist, J.; Miller, T. A. *Bioorg. Med. Chem. Lett.* **2008**, *18*, 973.
14. Wang, D.-F.; Helquist, P.; Wiech, N. L.; Wiest, O. *J. Med. Chem.* **2005**, *48*, 6939.
15. Nielsen, T. K.; Hildmann, C.; Dickmanns, A.; Shwienhorst, A.; Ficner, R. *J. Mol. Biol.* **2005**, *354*, 107.
16. Vannini, A.; Volpari, C.; Filocamo, G.; Casavola, E. C.; Brunetti, M.; Renzoni, D.; Chakravarty, P.; Paolini, C.; De Francesco, R.; Gallinari, P.; Steinkuehler, C.; Di Marco, S. *Proc. Natl. Acad. Sci. U.S.A.* **2004**, *101*, 1506.
17. KrennHrubic, K.; Marshall, B.; Hedglin, M.; Verdin, E.; Ulrich, S. M. *Bioorg. Med. Chem. Lett.* **2007**, *17*, 2874.
18. Dobler, M. R.; Grob, J. E.; Patnaik, A.; Radetich, B.; Shultz, M.; Zhu, Y. World Patent WO 2007038459 A2 20070405, 2007.
19. Balasubramanian, S.; Ramos, J.; Luo, W.; Sirisawad, M.; Verner, E.; Buggy, J. J. *Leukemia* **2008**, *22*, 1026.
20. Kim, H. J.; Bae, S. C. *Am. J. Transl. Res.* **2011**, *3*, 166.
21. Lemoine, M.; Younes, A. *Disc. Med.* **2010**, *10*, 462.
22. Dai, Y.; Chen, S.; Kramer, L. B.; Funk, V. L.; Dent, P.; Grant, S. *Clin. Cancer Res.* **2008**, *14*, 549.
23. Mann, B. S.; Johnson, J. R.; Cohen, M. H.; Justice, R.; Pazdur, R. *Oncologist* **2007**, *12*, 1247.
24. Hider, R. C.; Kong, X. *Nat. Prod. Rep.* **2010**, *27*, 637.
25. Monovich, L. G.; Tommasi, R. A.; Fujimoto, R. A.; Blancuzzi, V.; Clark, K.; Cornell, W. D.; Doti, R.; Doughty, J.; Fang, J.; Farley, D.; Fitt, J.; Ganu, V.; Goldberg, R.; Goldstein, R.; Lavoie, S.; Kulathila, R.; Macchia, W.; Parker, D. T.; Melton, R.; O'Byrne, E.; Pastor, G.; Pellas, T.; Quadros, E.; Reel, N.; Roland, D. M.; Sakane, Y.; Singh, H.; Skiles, J.; Somers, J.; Toscano, K.; Wigg, A.; Zhou, S.; Zhu, L.; Shieh, W. C.; Xue, S.; McQuire, L. W. *J. Med. Chem.* **2009**, *52*, 3523.
26. Sudarsan, N.; Cohen-Chalamish, S.; Nakamura, S.; Emilsson, G. M.; Breaker, R. R. *Chem. Biol.* **2005**, *12*, 1325.
27. Mueller, J. *Metallomics* **2010**, *2*, 318.
28. CSD. Cambridge Crystallographic Data Centre, Cambridge, UK.
29. Mareque Rivas, J. C.; Salvagni, E.; Parsons, S. *Chem. Commun.* **2004**, 460.
30. Ueda, E.; Yoshikawa, Y.; Kishimoto, N.; Tadokoro, M.; Sakurai, H.; Kajiwara, N.; Kojima, Y. *Bull. Chem. Soc. Jpn.* **2004**, *77*, 981.
31. Xie, Y.; Yu, Z.; Huang, X.; Wang, Z.; Niu, L.; Teng, M.; Li, J. *Chem. Eur. J.* **2007**, *13*, 9399.
32. Takayama, T.; Ohuchida, S.; Koike, Y.; Watanabe, M.; Hashizume, D.; Ohashi, Y. *Bull. Chem. Soc. Jpn.* **1996**, *69*, 1579.
33. Katsoulakou, E.; Giannis, X.; Papaefstathiou, S.; Konidaris, K. F.; Pairs, G.; Raptopoulou, C.; Cordopatis, P.; Manessi-Zoupa, E. *Polyhedron* **2009**, *28*, 3387.
34. Gantt, S. L.; Joseph, C. G.; Fierke, C. A. *J. Biol. Chem.* **2010**, *285*, 6036.
35. Dowling, D. P.; Gantt, S. L.; Gattis, S. G.; Fierke, C. A.; Christianson, D. W. *Biochemistry* **2008**, *47*, 13554.
36. Hunt, J. B.; Neece, S. H.; Schachman, H. K.; Ginsburg, A. *J. Biol. Chem.* **1984**, *259*, 14793.
37. Lim, J. W.; Oh, Y.; Kim, J.-H.; Oak, M.-H.; Na, Y.; Lee, J.-O.; Lee, W.-S.; Cho, H.; Park, K.-W.; Choi, H.; Kang, J. *Bioorg. Med. Chem. Lett.* **2010**, *20*, 2099.
38. Otwinowski, Z.; Minor, W. *Methods Enzymol.* **1997**, *276*, 307.
39. Storoni, L. C.; McCoy, A. J.; Read, R. J. *Acta Crystallogr., Sect. D* **2004**, *59*, 1145.
40. Brunger, A. T.; Adams, P. D.; Clore, G. M.; DeLano, W. L.; Gros, P.; Grosse-Kunstleve, R. W.; Jiang, J. S.; Kuszewski, J.; Nilges, N.; Pannu, N. S.; Read, R. J.; Rice, L. M.; Simonson, T.; Warren, G. L. *Acta Crystallogr., Sect. D* **1998**, *54*, 905.
41. Blanc, E.; Roversi, P.; Vonrhein, C.; Flensburg, C.; Lea, S. M.; Bricogne, G. *Acta Crystallogr., Sect. D* **2004**, *60*, 2219.
42. Emsley, P.; Cowton, K. *Acta Crystallogr., Sect. D* **2004**, *60*, 2126.
43. (a) PRIME, (b) Glide version 5.0, (c) SiteMap version 2.4. Maestro. Schrodinger Inc., Portland, OR.
44. Somoza, J. R.; Skene, R. J.; Katz, B. A.; Mol, C.; Ho, J.; Jennings, A. J.; Luong, C.; Arvai, A.; Buggy, J. J.; Chi, E.; Tang, J.; Sang, B.-C.; Verner, E.; Wynands, R.; Leahy, E. M.; Dougan, D. R.; Snell, G.; Navre, M.; Knuth, M. W.; Swanson, R. V.; McRee, D. E.; Tari, L. W. *Structure* **2004**, *12*, 1325.
45. Thompson, J. D.; Higgins, D. G.; Gibson, T. J. *Nucleic Acids Res.* **1994**, *22*, 4673.
46. Proasis2. Desert Scientific Software, Sydney, Australia.